ISSN : 0019-5693

INDIAN JOURNAL
OF
THEORETICAL PHYSICS

VOLUME 68 **NOS. 1,2**

JANUARY, 2020 – JUNE, 2020

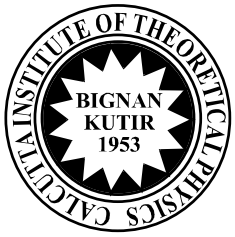

Published by the
CALCUTTA INSTITUTE OF THEORETICAL PHYSICS
(Formerly, INSTITUTE OF THEORETICAL PHYSICS)
"BIGNAN KUTIR"
4/1, MOHAN BAGAN LANE, KOLKATA-700004

(Peer-reviewed Journal)

ISSN : 0019-5693

INDIAN JOURNAL
OF
THEORETICAL PHYSICS

[Founder President : Late Prof. K. C. Kar, D. Sc.]

VOLUME 68 **NOS. 1,2**

JANUARY, 2020 – JUNE, 2020

Director : **J. K. Bhattacharjee**
Secretary : **S. K. Sarkar**

INDIAN JOURNAL
OF
THEORETICAL PHYSICS

"BIGNAN KUTIR"
4/1, MOHAN BAGAN LANE, KOLKATA-70004, INDIA

SUBSCRIPTION RATE

INDIA : For Library (Institute)

₹ 1500.00 for each volume

FOREIGN : $ 350 for each volume

Drafts, Orders, Enquiries & Claim for Non-Receipt of Journal should be sent to :

CALCUTTA INSTITUTE OF THEORETICAL PHYSICS
(Formerly, INSTITUTE OF THEORETICAL PHYSICS)
"BIGNAN KUTIR"
4/1, MOHAN BAGAN LANE, KOLKATA-700004, India

C O N T E N T S

INDIAN JOURNAL OF THEORETICAL PHYSICS, VOL 68, NOS. 1 & 2, 2020

Nature of Secondary Structural Alterations of Human Hemoglobin During Interactions With Gold Nanoparticle And Reduced Graphene Oxide

Madhurima Chakraborty[1] and Tapan Ganguly[2]

[1] Department of Biochemistry, West Bengal State University, Kolkata 700 126, India

[2]School of Laser Science and Engineering, Jadavpur University, Kolkata 700032, India

[2] Email: tapcla@rediffmail.com

[Abstract: Hemoglobin is a multi-subunit protein known to interact with small molecules of nano-dimensions. The study of such bimolecular interactions often provides knowledge regarding potential biomedical applications of nanoparticles. As such gold nanoparticle (GNP) and reduced graphene oxide (RGO) will be considered here for assessment of biocompatibility for effective applications in biological microenvironment particularly in terms of ability to alterprotein's secondary structure. The biocompatible nature of nanoparticles will be compared predominantly by the extent of alterations in secondary structure monitored by CD spectral analysis of clinically significant protein like Human Hemoglobin (HHb) and the comparative approach will be undertaken to gather knowledge regarding the better biocompatible nanoparticle for prospective biomedical applications. That is if the proteins retain its overall secondary structural features then the nanoparticles will act as a promising candidate for applications in biological micro-environment especially in the fields of drug delivery, biosensors, bio-imaging and others. Altogether our comparative approach

will suggest RGO to be the better candidate for effective biomedical applications compared to GNP in terms of their ability to alter secondary structure of HHb]

Keywords: Human Hemoglobin, Gold nanoparticle, Reduced Graphene Oxides, Secondary structure, CD spectra

1. Secondary structural features of HHb

HHb is a multi-subunit protein having two identical α and β subunits. The two identical α subunits are represented as A and C subunits and the two identical β subunits are represented as B and D subunits (Fig 1a). The predominant secondary structural feature in HHb is α-helix as evident in Fig 1b.HHb is already known to perform one of the vital functions in the body of carrying oxygen. Each subunit of HHb has a heme group that consists of protoporphyrin ring. A central Fe atom links the N atom of the four pyrrole rings of the protoporphyrin ring system within each hememoeity. The Fe atom of heme also connects with the protein part of HHb through the imidazole ring of Histidine. HHb as a multi-subunit protein not only has confined its function only as a carrier of oxygen but also is known to possess characteristics structural features to act as a model protein for interaction with small molecules of nano-dimensions[1-10].

a b

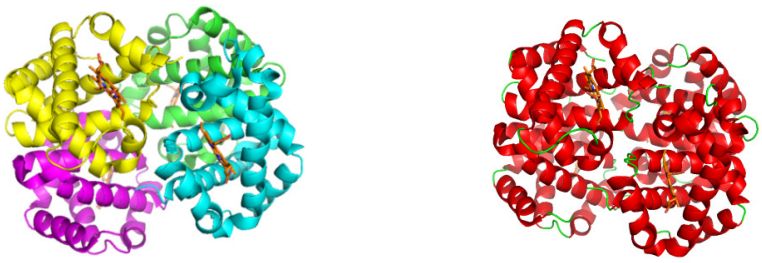

Figure 1

(a) Three dimensional structure of Human Hemoglobin (PDB ID- 2DN2), subunit A- green, B - cyan, D- yellow, D- magenta. (b) Secondary structural features of Human Hemoglobin (PDB ID- 2DN2), helix- red, sheet- yellow, loop- green, heme- orange.

2. Members of gold and carbon nano-family - GNP and RGO

Although there are many members present within the gold and carbon nano-family but our plan was to assess the biocompatible nature of two nanoparticles of different size and shape. They include GNP and RGO. GNPs have size around 18-20 nm and possess important properties like non-toxicity, solubility, chemical inertness, low cost[11-18] (Fig 2a). Besides, Swarnabhasma, a popular herbal medicine, was reported to comprise gold particles of micrometer and nanometer size. However in order to use GNPs extensively in biological milieu, the effect of GNP on secondary structure of proteins of clinical significance (HHb) must be considered.

Furthermore an oxidized derivative of graphene that forms two-dimensional (2D) carbon nanomaterial of single atom-thickness, GO, was chosen as the second member of carbon nano-family (Fig 2b). GO also exhibits outstanding physical and chemical properties that include increased surface area to volume ratio, conductivity and good mechanical property[19-23]. Not only that GO possesses oxygen-containing surface functional groups like carboxyl, epoxide and hydroxyl groups which heightens its wide-range of prospective functionality. Also when GO is reduced to RGO, some of the characteristics of GO are modified. The process of reduction may cause modification in characteristics like compatibility, solubility in a biological system and interaction properties.

The modification occurs possibly due to variation in exposed functional groups on GO and that of RGO.

Accordingly both the nanoparticles can be utilized for potential biomedical applications(development of drug delivery and biosensors, bio-imaging, disease diagnosis and treatment of diseases like cancer, molecular recognition, molecular medicine and others) if they appear to be biocompatible. One of the simplest and convenient ways is to check the extent of secondary structural alterations of proteins upon interactions with nanoparticles. Thus we focus on the comparison of nature of alterations of secondary structure of HHb upon interactions with GNP and RGO. If significant alterations in secondary structural features are not observed in HHb in spite of interactions with GNP and RGO, then the nanoparticles can be taken into consideration for extensive biomedical applications within biological micro-environment.

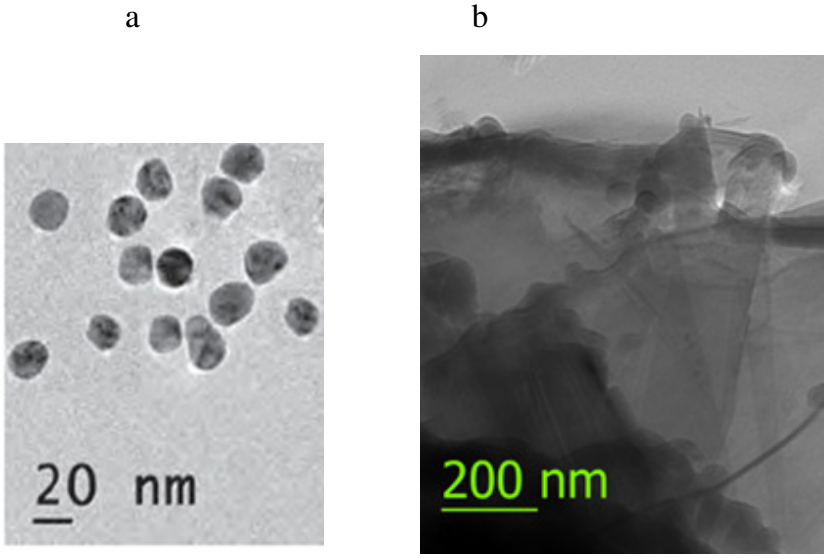

Figure 2

(a) HRTEM image of GNP (modified from 1). (b) HRTEM image of GO (modified from 2).

3. Secondary structural alterations of HHb in presence of GNP

In order to assess the secondary structural changes of HHb upon interaction with GNP, CD spectral analysis of HHb has been discussed[1-3, 24-30] (Fig 3). The equation applied to state the secondary structural observations from CD spectroscopy in terms of mean residue ellipticity (MRE) (degree cm^2 mol^{-1}) has been given below,

$$[\theta_\lambda] = \frac{\theta}{10nlc} \quad \ldots (1)$$

In the equation, c denotes concentration of protein (g/ml), θ signifies observed rotation (degree), l designates path length (cm) and n implies number of amino acid residues present in HHb (574 residues).

Furthermore in order to evaluate the percentage of α-helicity in HHb in presence of GNP, the following equations are used

$$\%\ of\ \alpha - helix = \frac{-[\theta]_{208} - 4000}{33000 - 4000} \quad \ldots (2)$$

$$\%\ of\ \alpha - helix = \frac{[\theta]_{222} + 2340}{-30300} \quad \ldots (3)$$

As observed in Fig. 3, negative peaks were noticed near 208 and 222 nm. The singlet electronic transitions in the backbone peptide bond of a protein occur at 190 nm and 220 nm originated from the amide chromophore $N - C = O$. 220 nm transition arises from the lone pair on oxygen to a π^*antibonding orbital ($n\pi^*$ transition) and 190 nm transition originates from a non-bonding π orbital to the π^* orbital ($\pi\pi^*$ transition). These two transitions mix in the chiral environment of the protein and yield the different spectra corresponding to the different secondary structural element present within the protein[31,32]. Exciton splitting of the $\pi\pi^*$ transition produces positive peak at 190 nm (not shown in the figures) and 208 nm having negative peak due to α- helix

along with a negative 220 nm peak originating from the $n\pi^*$ transition. The peaks at those regions of 208 nm to 220 nm of CD spectra appeared to be the signature peaks for the presence of α-helicity within the protein[1-3]. The change in % α-helicity of HHb upon interaction with GNP has been summarized in Table 1a and b. As evident in Table 1a, the % α-helicity (negative band at ~ 208 nm) decreased by ~ 5.44 % upon interaction with GNP. The % α-helicity(negative band at ~ 222 nm) decreased slightly by ~ 6.07 % upon interaction with GNP (Table 1b). Therefore the observations apparently suggested minor changes in CD spectra of HHb at 208 nm and 222 nm upon interaction with GNP. In other words HHb retained its overall secondary structure even after interaction with GNP. Thus GNP can be used as a biocompatible nanoparticle for use in biological micro-environment especially as drug-delivery system, biosensors, bio-imaging and others.

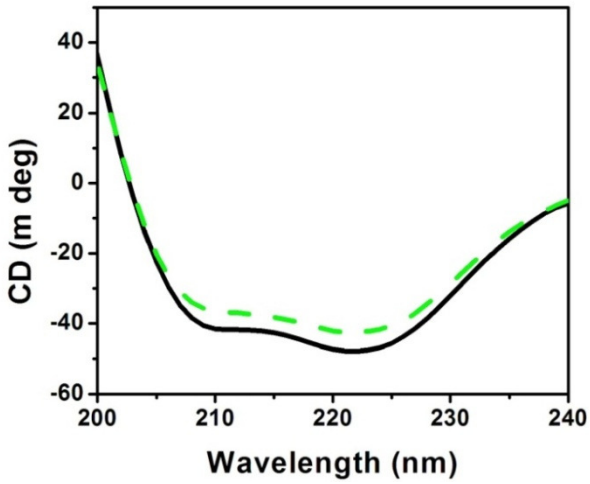

Figure **3**

CD spectra of HHb in absence (black) and presence (7.5 x 10^{-6} M) of GNP (green).Modified from Ref.1.

4. Secondary structural alterations of HHb in presence of RGO

Moreover the α-helicity of HHb is also monitored in presence of RGO. As observed in Fig.4, negative bands at about 209 and 220 nm have been observed due to occurrence of α-helical secondary structure within HHb. The change in % α-helicity of HHb upon interaction with RGO has been summarized in Table 1a and b. As observed the % α-helicity at both the regions mentioned above was observed to alter slightly. Precisely, the percentage of α-helicity of HHb,upon interaction with RGO, increased slightly, by only ~ 1.14 %, at 209 nm (Table 1a). Also, the % of α–helix content of HHb, in presence of RGO, increased minutely by ~ 0.55 %, at 220 nm (Table 1b). The observations thus indicated minor alterations in CD spectral bands corresponding to α-helicity of HHb even after interaction with RGO. Thus the overall structure of HHb was apparently retained in presence of RGO. Thus RGO can act as biocompatible member of carbon nano-family for prospective biomedical application within biological microenvironment.

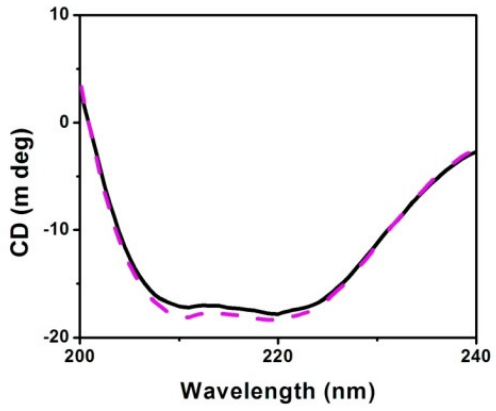

Figure 4

CD spectra of HHb in absence (black) and presence 5 μg/ml of RGO (magenta).Modified from Ref 2.

Table 1a

Change in % α-helicity near 208 nm of HHb upon interaction with GNP and RGO

Sample	% change in α-helicity near 208 nm
HHb-GNP	Decrease by 5.44
HHb-RGO	Increase by 1.14

Table 1b

Change in % α-helicity near 222 nm of HHb upon interaction with GNP and RGO

Sample	% change in α-helicity near 222 nm
HHb-GNP	Decrease by 6.07
HHb-RGO	Increase by 0.55

5. Comparative approach towards alteration of secondary structure of HHb upon interaction with GNP and RGO

The present review focused on the alteration of CD spectral bands of HHb upon interaction with members of carbon and gold nano-family. Minor changes in % α-helicity of HHb were observed to occur in presence of GNP and RGO. Thus, even after interaction with GNP and RGO, the overall secondary structure of HHb, was nearly retained. Apparently the biocompatible nature of GNP and RGO was compared for better understanding (Table 2). The comparative approach suggested lesser changes (less than 1.5 %) in % α-helicity of HHb in presence of RGO compared to GNP (more than 6 %). Since the % change in α-

helicity appeared to be more for GNP and less for RGO, thus RGO possibly acts as a promising member of carbon nano-family for its use as drug delivery system, biosensors and others within biological micro-environment.

Table 2

Comparison of % change α-helicity of HHb upon interaction with GNP and RGO

Protein	Nanoparticles	Maximum % change α-helicity of HHb
HHB	GNP	More than 6 %
	RGO	Less than 1.5 %

Acknowledgement

TG gratefully acknowledges the University grant commission (UGC), New Delhi, India for awarding Emeritus fellowship and contingency grant (F.6-6/2014-15/EMERITUS-2014-15-GEN-3976) forresearch purposes. We express sincere gratitude to Dr. Bibhutibhusan Show of Department of Chemistry, Jadavpur University for extending his help in performing CD spectroscopic experiments. Special thanks to Ayan Mallick and Prof. Pabitra K. Chakrabarti for synthesis of RGO and Dr. Munmun Bardhan for synthesis of GNP.

References

1. Chakraborty M., Paul S., Mitra I., Bardhan M., Bose M., Saha A., Ganguly T., Journal of Photochemistry & Photobiology, B: Biology, **178,** 355–366, (2018).

2. Chakraborty M., Mitra I., Roy A. J., Paul S., Mallick A., Das S., Saha A., Show B., Chakrabarti P. K., Ganguly T.. Spectrochimica Acta Part A, **247**, 119079, (2021).
3. Chakraborty M., Mitra I., Sarkar Bardhan K., M., Paul S., Basu S., Goswami A., Saha A., Show B., Ganguly T., Spectrochim. Acta Part A , **215** 313–326(2019).
4. Mandal P., Ganguly T., J. Phys. Chem. B, **113,**14904–14913 (2009).
5. G. Mandal, S. Bhattacharya, T. Ganguly, J Appl Phys, **110**, 024701-024708 (2011).
6. Martin D.W., Mayes P.A., Rodwell V.W., Harper's Review of Biochemistry, 19thed., LMP, New York, **1983**.
7. Liu C.W., Bo A. L, Cheng G.J., Lin X.Q., Dong S.J., Biochim. Biophys.Acta, **1385,** 53–60 (1998).
8. Sil S., Kar M., Chakraborti A.S., Photochem J.. Photobiol. Biol B, **41,** 67–72 (1997).
9. De S., Girigoswami A., J. Colloid Interf. Sci, **296,** 324–331 (2006).
10. Shen X.-C., Liou X.-Y., Ye L.-P., Liang H., Wang Z.-Y., J. ColloidInterf. Sci, **311,** 400–406 (2007).
11. Pal G., Paul A., Yadav S., Bardhan M., De A., Chowdhury J., Jana A., Ganguly T., Nanosci Nanotechnol J, **15,** 5775-5784 (2015).
12. Eustis S. and El-Sayed M. A., Chem. Soc. Rev. **35,** 209-217 (2006).
13. Cobley C. M., Chen J., Cho E. C., Wang L. V., and Xia Y., Chem. Soc. Rev. **40,** 44-56 (2011).
14. Ming T., Kou X. S., Chen H. J., Wang T., Tam H. L., Cheah K. W., Chen J. Y., and Wang J. F., Angew Chem. Int Ed, **47,** 9685-90 (2008).
15. Li C., Fan F., Yin B., Chen L., Ganguly T., and Tian Z. Q., NanoResearch, **6,** 29-37 (2013).
16. Soppimath K. S. and Betageri G., Wiley John & SonsInc, New York (2008).
17. Pellequer Y. and Lamprecht A., Pan Stanford Publishing Pte. Ltd., Singapore, p. 93 (2009).

18. Sur U. K., Mandal G., and Ganguly T., Nanosci. Nanotechnol. An Indian Jour. **6**, 104-107 (2012).
19. Choi W., Lahiri I., Seelaboyina R., Kang Y.S., Crit. Rev. Solid State Mater. Sci, **35** (1) 52–71(2010).
20. Wei X.L., Ge Z.Q., Carbon, **60,** 401–409 (2013).
21. Priyadarsini S., Mohanty S., Mukherjee S., Basu S., Mishra M., J NanostructChem, **8**, 123–137 (2018).
22. Geim A.K., Novoselov K.S., Nature Mater, **6**(3) 183 (2007).
23. Sanchez V.C., Jachak A., Hurt R.H., Kane A.B., Chem. Res. Toxicol, 25(1) 15–34, (2011).
24. Mahato M., Pal P., Kamilya T., Sarkar R., Chaudhuri A., G.B., Talapatra J. Phys. Chem. B, **114,** 7062–7070 (2010).
25. Mandal P., Bardhan M. and Ganguly T., J Photochem Photobiol B: Biology, **99,** 78–86 (2010).
26. Mahato M., Pal P., Tah B., Ghosh M., Talapatra G. B., Colloids and Surfaces B: Biointerfaces, **88,** 141– 149 (2011).
27. Chen Y. H., Yang J. T., Martinez H. M., Biochemistry, **11,** 4120–4131 (1972).
28. Sreerama N., Woody R. W., Anal. Biochem, **287**, 252–260 (2000).
29. Lu Z.X., Cui T., Shi Q.L., first ed., Science Press, (1987).
30. Bhunia A. K., Kamilya T., Saha S., Nano Convergence, 4:28 (2017).
31. Chakraborty M., Ganguly T., Karnatak University Journal of Science **51,** 28-39 (2020).
32. Singha S., Bose P P, Ganguly T, Campana P, T. R, Chatterjee B P Chatterjee, J Luminescence, **160,** 119-127 (2015).

INDIAN JOURNAL OF THEORETICAL PHYSICS, VOL 68, NOS. 1 & 2, 2020

A Comparative Study Between Dst And SYM-H Indices Based On Pattern Identification

Amaresh Bej, Adrija Banerjee*

Department of Physics, Indian Institute of Engineering Science and Technology, Shibpur, P.O. - Botanic Garden, Howrah – 711103, West Bengal, India.

E-mail: adrija_bnrj@yahoo.co.in

T. N. Chatterjee

Department of Electronics, Dinabandhu Andrews College, 54, Raja S.C. Mullick Road, Garia, Kolkata 700084, West Bengal, India.

and

Abhijit Majumdar

Department of Physics, Indian Institute of Engineering Science and Technology, Shibpur, P.O. - Botanic Garden, Howrah – 711103, West Bengal, India.

[Abstract: Dst and SYM-H indices are two different measurements of the geomagnetic storm. SYM-H index is a high-resolution version of the traditional Dst index, though there are some differences in their measurement techniques. A detailed understanding of the complex structure of the traditional Dst index along with the SYM-H index is extremely important to forecast the onset of the

* Address for correspondence

geomagnetic storm to prevent huge monetary losses and unnecessary hazards in northern hemisphere countries like U.S., Canada, or northern Europe. Like any other time series, these two geomagnetic indices are also a combination of different patterns. Identifying and comparing the extracted patterns from the two indices is an alternative approach to understand the gesture of their hidden layers. In this paper, a composite method involving adaptive delta modulation, optimum state space reconstruction, and pattern identification is presented to investigate the proximity between the Dst and SYM-H indices. The results clearly indicate some significant insight into the underlying intricate structure of the two indices.]

Key-words: Solar wind-magnetosphere interactions, Dst index, SYM-H index, Time series analysis, pattern recognition.

1. Introduction

The disturbance storm time (Dst) index is an indication of the geomagnetic activities in the terrestrial magnetosphere and is computed based on the average value of the horizontal component of the Earth's magnetic field recorded at four different observatories, namely Hermanus (34.42°S, 19.22°E in geographic latitude and longitude), Kakioka (36.23°N, 140.19°E), Honolulu (21.32°N, 158°W), and San Juan (18.11°N, 66.15°W). To nullify the influence of the auroral effect as much as possible, these stations are evenly spaced in longitude and near enough to the magnetic equator. Again, to minimize the influence of the equatorial electrojet current flowing in the ionosphere, they are placed at a significant distance away from the magnetic equator[1]. However, the SYM-H index is a more frequently measured geomagnetic index than the traditional Dst index. Although it

is widely considered as the higher-resolution version of the classic Dst index and is measured in nT in a similar fashion, it differs from the traditional index in several ways: in terms of resolution, the difference between the number of observatories of the two indices[1], consideration of one station from each pair of stations in case of SYM-H index[2], determination of the base value at each station[3], the effect of the tail current[4], removal of Solar quiet daily variation, Sq, for each station[5], and the difference of induced magnetic fields due to geologic conductivity structures beneath the stations[6]. The magnetometer stations used to record the ground data for the calculation of SYM-H are San Juan (18.11°N, 66.15°W), Fredericksburg (38.21°N, 77.37°W), Boulder (40.14°N, 105.24°W), Tucson (32.17°N, 110.73°W), Honolulu (21.32°N, 158°W), Memambetsu (43.91°N, 144.19°E), Urumqi (44.36°N, 86.94°E), Alibag (18.64°N, 72.87°E), Martin de Vivies (37.8°S, 77.57°E), Hermanus (34.42°S, 19.22°E), and Chambon-la-Foret (48.02°N, 2.26°E). For each month, the data from six of the above stations are selected based on the availability and the quality of the recorded data. As the selection of Honolulu and Memambetsu are fixed for each month, the other four stations are selected one from each of the set, Boulder or Tucson, Fredericksburg or San Juan, Hermanus or Chambon-la-Foret, Alibag or Martin de Vivies or Urumqi[1,2]. A detailed description of the mathematical method involving the derivation of the SYM-H index can be found in Iyemori T. et al.[3].

For several past years, pattern recognition became a widely used technique to study and analyze the existing regularities in an otherwise complex time series. A significant number of studies had been done applying the pattern recognition method in the geomagnetic storm[7] while,

in general, the artificial Neural Network approach too had presented some notable works[8,9]. The study involving the investigation of the inherent structure of the SYM-H index is still quite unexplored, though few excellent papers had been devoted in recent years involving the analysis, characterization, and multifractal modeling of SYM-H index[10,11,12] and also predicting the SYM-H index from solar wind and IMF data using the NARX neural network[13].

The dynamical characteristics of these two geomagnetic indices primarily depend on their intricate and complex structure which can be regarded as a combination of various overlapping patterns. Thus, it is necessary to inspect and unfold these distinguished patterns to gain an insight into these indices and to compare their structural properties. In the current paper, we proposed an analytical method to compare Dst and SYM-H indices on the basis of pattern recognition. The method is a composite one, involving the steps: (1) Converting the geomagnetic index series to its binary form using the delta modulation technique with limited adaptivity, (2) construction of the optimum state space of the series, (3) identification of the complete set of patterns hidden in the series, and (4) finally characterization of the structural dynamics of the series.

2. Data

Here we used the 1-hour Dst data and 5-min SYM-H data from the year 1997 to the year 2007 as extracted from NASA/GSFC's OMNI data set through OMNIWeb. The OMNI data were obtained from the GSFC/SPDF OMNIWeb interface at http://omniweb.gsfc.nasa.gov[14].

3. Method

To convert the Dst and the SYM-H indices data from analog to digital form, the delta modulation with limited adaptivity technique had been applied that can be regarded as a 1-bit differential pulse code modulation (DPCM) scheme. A reference signal is initiated, the analog signal is sampled and then by comparing the reference signal with the input signal, the increase or decrease in relative amplitude is determined. A step size (Δ) is predefined for each sampler where,

$$\Delta_I = K_I \times \sigma_D \times 2^d \text{ for } 0 \leq d \leq 2 \quad \text{... (1)}$$

$$\Delta_D = K_D \times \sigma_D \times 2^d \text{ for } 0 \leq d \leq 2 \quad \text{... (2)}$$

Here, K_I and K_D are two constants and σ_D is the standard deviation of the absolute differential values of the input series $X_i(t)$. In equations 1 and 2, the value of d is limited to only three values, 0, 1, and 2. If the increment (decrement) between the two terms, $X_i(t)$ and $X_r(t-1)$ continues for three consecutive steps, the value of d becomes 0,1, and 2 for the first, second, and third step, respectively. But, if the fourth consecutive step also shows an increment (decrement), the value of d is still 2 and remains so for any further consecutive increments (decrements). Whenever there is a decrement (increment) in the next step, the value of d is reset to 0. As the reference signal $X_r(t)$ has been formed, the delta-modulated 1-bit binary string output series $Y_{dm}(t)$ is computed using the equations:

$$Y_{dm}(t) = 1 \text{ for } X_r(t+1) \geq X_r(t) \quad \text{... (3)}$$

$$Y_{dm}(t) = 0 \text{ for } X_r(t+1) < X_r(t) \quad \text{... (4)}$$

Now, by the sliding window technique, the number of occurrences of all possible 2^m binary patterns in the series $Y_{dm}(t)$ is determined for the value of m = 2 onwards up to a considerable value. A database is formed for

different values of m and each of them contains a 2^m number of patterns including their respective number of occurrences in the series $Y_{dm}(t)$.

In his 2001 paper, Chatterjee[15] discussed the reconstruction of the optimum state space in detail. Being faithful to his work, we too consider that specified technique to be fruitful enough for our present analysis. The correlation sum $C(r, m, N)$ is calculated which is a function of the Hamming distance r, dimension m, and a total number of data N and is expressed as:

$$C(r, m, N) = \frac{1}{2^{m-1}} \sum_{j=1}^{N} G_j(r) \quad \ldots (5)$$

If the number of occurrences of the pattern having $D_0 = 0$ is O_0 and $D_0 = 1$ is O_1, the expectation, $G_j(r)$, of D_0 to be appeared as '1' over '0' is:

$$G_j(r) = \left[\frac{O_1}{O_0 + O_1} - 0.5\right]^2 \quad \ldots (6)$$

In this way, the expectations $G_j(r)$ are calculated for all sets of patterns in the database obtained from the sliding window technique, and $C(r, m, N)$ is calculated accordingly. At a particular point of $m = M$, where the $C(r, m, N)$ is maximum, the optimum state space is achieved beyond which no further information is available.

As M is estimated, the entire delta modulated binary data series is then thoroughly searched for all the 2^M patterns. The number of occurrences of each pattern is recorded. A graph for the number of occurrences versus each pattern is plotted to find the pattern having the maximum number of occurrences and also the pattern having zero or the minimum number of occurrences in the modulated series. Moreover, a histogram of power-law degree distribution is plotted in a log-log scale,

an exponential trend line is fitted to the histogram and the slope γ is calculated which is inversely proportional with the metric entropy of the system and directly proportional to the predictability time. The value of the information content γ will be $\gamma = \infty$ for a regular system, $\gamma = 0$ for a truly random system, and $0 < \gamma < \infty$ for a chaotic system.

4. Result and Discussion

The actual waveforms and patterns of the geomagnetic indices signals are nearly impossible to extract from their analog form due to the different scale factors enfolded in different parts of the time series. Converting the time series into a digital signal makes the inspection much easier by revealing the hidden information concealed in their intricate structures and the Differential Pulse code modulation technique (DPCM) is the most suitable way of conversion. The value of the increment coefficients K_I are 0.54 and 0.55 and the decrement coefficients K_D are 1.3 and 1.1 respectively for the 1-hour Dst and 5-min SYM-H index data series for each year of the entire 23rd solar cycle.

Now, once the binary data are obtained, we find the number of occurrences of a pattern by sliding window technique for the modulated Dst as well as SYM-H index for all values of m ranged between 2 to 16 for the entire 23rd solar cycle. The correlation sum $C(r, m, N)$ is calculated for each value of m and the optimum state spaces are achieved for dimension $M = 10$ for the Dst index and $M = 14$ for the SYM-H index, respectively. It signifies that no new information can be retrieved from the modulated data series beyond this particular point of optimum state space. The higher value of the optimum state space for the 5-min

SYM-H index is indicating the presence of more information content than the hourly Dst index, owing to its higher resolution and larger dataset.

The highest possible combinations of binary string for Dst index is 1024 (as $2^M = 1024$, where M = 10) whereas for SYM-H index it is 16384 (as $2^M = 16384$, where M = 14). For both series, all the possible combinations of the binary strings are added sequentially for 11 years and are plotted in Figure 1 to illustrate the binomial degree distribution. The similar nature of the two graphs is quite obvious from careful observation of the figure, indicating the occurrences of identical sample patterns in a proportionate way in both series.

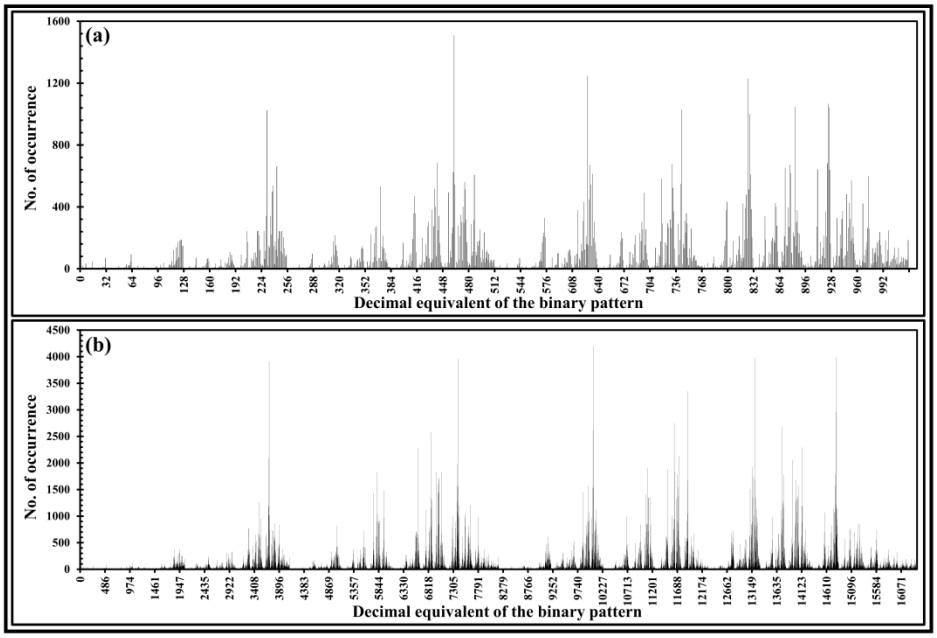

Figure 1

(a) A binomial degree distribution of the 11 years occurrences is plotted for the Dst index and **(b)** the same is plotted for the 5-min SYM-H index.

In the next step, for both the cases and for each year, the yearly no. of occurrences of a specific pattern in a series are sorted in a descending manner and are plotted in a log-log degree distribution graph. A power law is fitted in the plot and the estimated values of the power-law exponent γ are shown in Table 1 for all the 11 years of the solar cycle. Figure 2 demonstrates the log-log plot of the degree distribution of the patterns for both the 1-hour Dst and 5-min SYM-H indices for the year 2004. As seen from the Figure, the value of γ is γ = -6.17E-03 ± 3.54E-05 for 1-hour Dst index and γ = -3.70E-04 ± 9.28E-07 for 5-min SYM-H index.

Table 1

The percentage of absent patterns and the value of exponent γ obtained from the power-law degree distribution of occurrence of patterns for both 1-hour Dst and 5-min SYM-H indices for the entire 23rd solar cycle.

Year	Dst (1-hour)		SYM-H (5-min)	
	Absent pattern (%)	**γ**	**Absent pattern (%)**	**γ**
1997	23.9258	-5.40E-03 ± 2.48E-05	33.0444	-3.68E-04 ± 8.34E-07
1998	23.0469	-5.25E-03 ± 2.56E-05	33.8928	-3.70E-04 ± 9.66E-07
1999	28.1250	-5.68E-03 ± 2.76E-05	32.6355	-3.64E-04 ± 9.08E-07
2000	27.7344	-5.83E-03 ± 3.92E-05	37.4695	-3.95E-04 ± 1.31E-06
2001	31.4453	-6.16E-03 ± 4.37E-05	41.0217	-4.24E-04 ± 1.43E-06
2002	22.4609	-5.25E-03 ± 2.31E-05	31.2805	-3.49E-04 ± 8.15E-07
2003	29.9805	-6.18E-03 ± 3.70E-05	35.9192	-3.83E-04 ± 9.53E-07
2004	31.3477	-6.17E-03 ± 3.54E-05	33.6609	-3.70E-04 ± 9.28E-07
2005	30.7617	-6.17E-03 ± 4.62E-05	36.2915	-3.86E-04 ± 1.15E-06
2006	25.5859	-5.46E-03 ± 2.71E-05	31.5186	-3.54E-04 ± 8.80E-07
2007	23.3398	-5.35E-03 ± 2.44E-05	31.5979	-3.56E-04 ± 8.42E-07

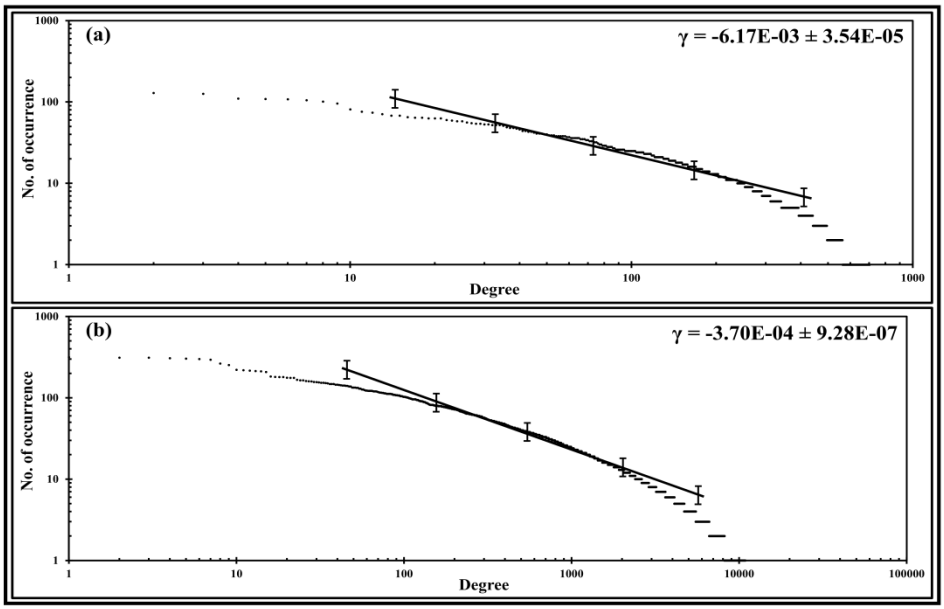

Figure 2

The log-log power-law degree distribution of the patterns found in **(a)** 1-hour Dst index and **(b)** 5-min SYM-H index for the year 2004.

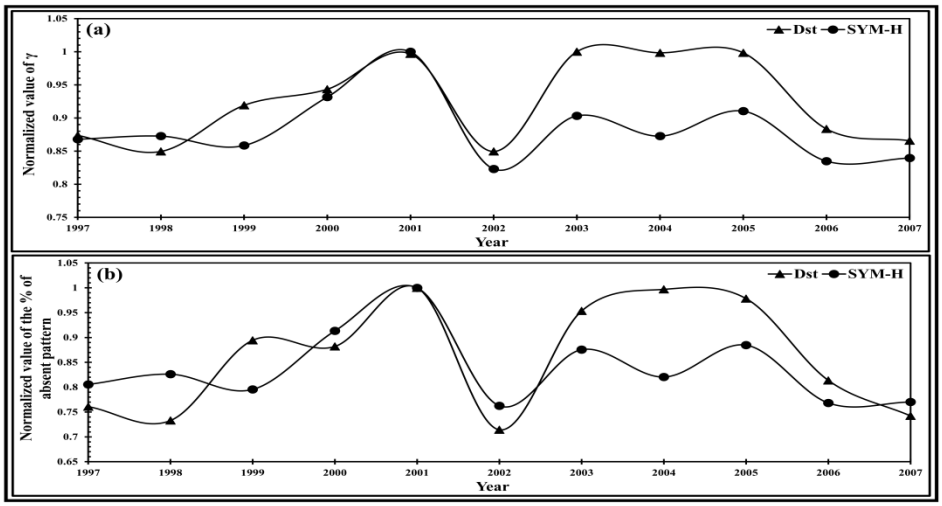

Figure 3

(a) The normalized value of the exponent γ and **(b)** The normalized value of the percentage of absent pattern for 1-hour Dst and 5-min SYM-H indices for the entire 23rd solar cycle.

Finally, Figure 3 illustrates the plots of the normalized value of the exponent γ and the normalized value of the percentage of absent patterns, respectively, for the period of the year 1997 to 2007 for both the series. As seen from each of the graphs, both the plots associated with Dst and SYM-H data follow nearly similar waveforms having significant values of the correlation coefficient between the plots, in Figure 3(a) it is 0.6978 and in Figure 3(b) it is 0.6847. These observations can be explained in such a way that the information contents for both the series vary with each year in a quite similar pattern while the SYM-H series, being the higher resolution one and having a large dataset, displays lower values in both the cases of values γ and the percentage of absent patterns in almost every year.

5. Conclusion

Both the Dst and SYM-H indices are measurements of geomagnetic activities on Earth and are widely used to indicate the intensity and occurrence of geomagnetic storms. The SYM-H index is considered as the higher-resolution version of the conventional Dst index though having a few inequalities in properties when extracting and analyzing their pattern in the technique stated in this paper. Observation from the results reveals many significant points:

1. The optimum value of the correlation sum C(r, m, N) is different for both the geomagnetic indices as the information content is different due to their resolution. The 5-min SYM-H index having a better resolution than the 1-hour Dst index exhibits a better capturing of the variation in the solar storm and solar wind dynamic pressure variations.

2. Both the series are composite combinations of multiple repeating, non-repeating, and never occurred patterns. The repeating patterns represent a high degree of predictability of the M^{th} data of the series from its previous (M-1) data, whereas the never occurred pattern also has great significance due to its definite non-existence.
3. It is also observed that the recognized patterns are almost uniform for both the geomagnetic indices series which indicates the same dynamical property between the series.
4. The absolute value of exponent γ ranged between 0 and ∞, obtained from the power-law degree distribution graph for both the indices indicates the presence of long-range correlation into the series.
5. The higher absolute value of exponent γ signifies more the presence of more periodic patterns whereas, the smaller value indicates randomness. The different values of exponent γ seen in the result denotes the difference in the dynamical property, the information content, and the scope of predictability. The similarity in the progression of the percentages of absent patterns concerning the exponent γ also acknowledges the same dynamical behavior and predictability for the entire 23^{rd} solar cycle.

The current study is a first-order approach to investigate these patterns through an alternate technique. The probability of occurrence of individual patterns can be calculated and included in the library of a model that can reliably predict future data. Also, the pattern set obtained around the storm time and quiet time can be analyzed separately to find any specific characteristics and hence to appropriately estimate the intensity and occurrence of the storm.

Reference

1. Wanliss, J. A., and K. M. Showalter, High-resolution global storm index: Dst versus SYM-H, J. Geophys. Res., **111**, A02202, doi:10.1029/2005JA011034, (2006).
2. Wanliss, J. A., When is it alright to use SYM-H as a storm index?, American Geophysical Union, Fall Meeting (2007), abstract id.SM32A-05 (2007).
3. Iyemori, T., Takeda, M., Nose, M., Odagi, Y. and Toh, H. Mid-latitude Geomagnetic Indices" ASY" and" SYM" for 2009 (Provisional). Data Analysis Center for Geomagnetism and Space Magnetism, Graduate School of Science, Kyoto University, Japan (2010).
4. Turner, N. E., Baker, D. N., Pulkkinen, T. I., and McPherron, R. L. Evaluation of the tail current contribution to Dst, J. Geophys. Res., **105**(A3), 5431– 5439, doi:10.1029/1999JA000248(2000).
5. Sugiura, M., and T. Kamei, Equatorial DST index 1957–1986, in IAGA Bull. 40, edited by A. Berthelier, and M. Menvielle, Int. Serv. of Geomagn. Indices Publ. Off., Saint Maur, France (1991).
6. Wanliss, J. A., and L. A. G. Antoine , Geomagnetic micropulsations: Implications for high resolution aeromagnetic surveys, Explor. Geophys., **26,** 535 doi: 10.1071/EG995535 (1995).
7. Chen, J., Cargill, P. J., and Palmadesso, P. J. , Predicting solar wind structures and their geoeffectiveness, J. Geophys. Res., **102** (A7), 14701– 14720, doi:10.1029/97JA00936 (1997).
8. Amata, E., G. Pallocchia, G. Consolini, M. F. Marcucci, and I. Bertello, Comparison between three algorithms for Dst predictions over the 2003–2005 period, J. Atmos. Sol. Terr. Phys., **70,** 496–502(2008).
9. Barkhatov, N.A., Bellustin, N.S., Levitin, A.E. et al. Comparison of efficiency of artificial neural networks for forecasting the geomagnetic activity index Dst. Radiophys Quantum Electron **43**, 347–355 (2000). https://doi.org/10.1007/BF02677150.

10. Wanliss, J.A. Nonlinear variability of SYM-H over two solar cycles. Earth Planet Sp **56,** e13–e16 (2004). https://doi.org/ 10.1186/BF03352507.
11. Wanliss, J. A. , Fractal properties of SYM-H during quiet and active times, J. Geophys. Res., **110,** A03202, doi:10.1029/ 2004JA010544 (2005).
12. Wanliss, J. A., and J. M. Weygand, Power law burst lifetime distribution of the SYM-H index, Geophys. Res. Lett., **34,** L04107, doi:10.1029/2006GL028235 (2007).
13. Bhaskar, A. and Vichare, G. Forecasting of SYMH and ASYH indices for geomagnetic storms of solar cycle 24 including St. Patrick's Day, 2015 storm using NARX neural network. Journal of Space Weather and Space Climate, **9,** p.A12. doi: 10.1051/swsc/ 2019007 (2019).
14. King, J. H., & Papitashvili, N. E., Solar wind spatial scales in and comparisons of hourly Wind and ACE plasma and magnetic field data. Journal of Geophysical Research**, 110,** A02209. https://doi.org/ 10.1029/2004JA010649 (2005).
15. Chatterjee, T.N., On the application of information theory to the optimum state-space reconstruction of the short-term solar radio flux (10.7cm), and its prediction via a neural network. Monthly Notices of the Royal Astronomical Society, **323**: 101-108. doi:10.1046/j.1365-8711.2001.04110.x (2001),.

———————

INDIAN JOURNAL OF THEORETICAL PHYSICS, VOL 68, NOS. 1 & 2, 2020

Design And Analysis of Chaotic Oscillator Using Chua's Circuit

Pratyusha Biswas Deb

Department of Electrical Engineering, Narula Institute Of Technology, Agarpara, Kol-700109, WB

Indranil Bhattacharyya*, Partha Sarathi Majumdar

Department of Physics, AcharyaPrafullaChandra College, New Barrackpore, Kol-700131, WB

Bikas Sarkar

Department of Physics, M.D. Mahavidyapith, Birati, Kolkata-700051, Kol-700051, WB

Sukriti Ghosh

Department of Physics, ShibpurDinobondhoo Institution (Coll), Howrah, WB

Soumya Das

S. M. Technologies Infra Pvt. Ltd; Kolkata-700001, WB

*Corresponding author: indranil@apccollege.ac.in

[**Abstract**: The present work is based on Leon Chua's observation on construction of a simpler circuit which would not be governed by the Lorentz equations, but would still give rise to chaotic behaviour. Using MATLAB ODE45 it is shown that Chua's circuit can be physically decomposed into a sinusoidal oscillator coupled witha voltage controlled nonlinear resistor. In particular, the passive LC tank resonator can be replaced by a general second order sinusoidal

oscillator, such as the Wien-bridge oscillator or even a third order such as the Twin T oscillator.Moreover,the chaotic nature of Chua's circuit has been realized and those parameters which produced chaos in the oscillator are checked by varying the values of those parameters up to which the oscillator shows its chaotic nature.]

Keywords: Chaotic, Oscillator, Polyester capacitors, LC tank resonant, twin T oscillator

1. Introduction

Until recently, very few chaotic oscillators existed in literature. This was a consequence of the fact that it was not clear how such strongly nonlinear circuits could be designed to produce chaos. The key word in this problem formulation is "Chaotic"[1]. The ordinary usage of the wordchaotic implies complete disorder –like tossing of a coin which might be a perfect example as no one can predict the outcome i.e. head or tail. However, from a scientific perspective such a system is rather trivial as we can easily quantify the different outcomes as equally probable and there is no possibility to produce more sophisticated predictions. We call these systems stochastic[2] in contrast to the predictable ones which are labelled deterministic. The present concept was first formulated by Chuaand Lin[3] to fabricate a simpler circuit that would not be governed by Lorentz equation[4] but would still give rise to chaotic behaviour. The present work is based on Chua's circuit which can be physically decomposed into a sinusoidal oscillator coupledwith a voltage controlled nonlinear resistor. In particular, the passive LC tank resonator can be replaced by a general second order sinusoidal oscillator, such as the Wien bridge oscillator or even a third order one such as twin T oscillator[5].

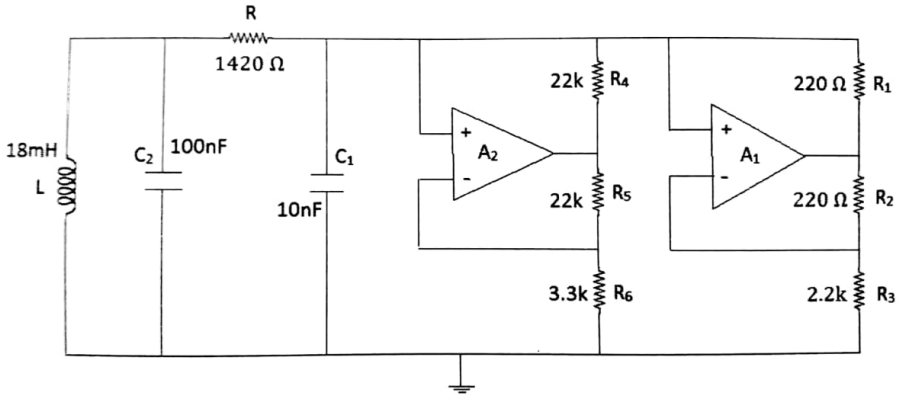

Figure 1

Practical Chua's Circuit

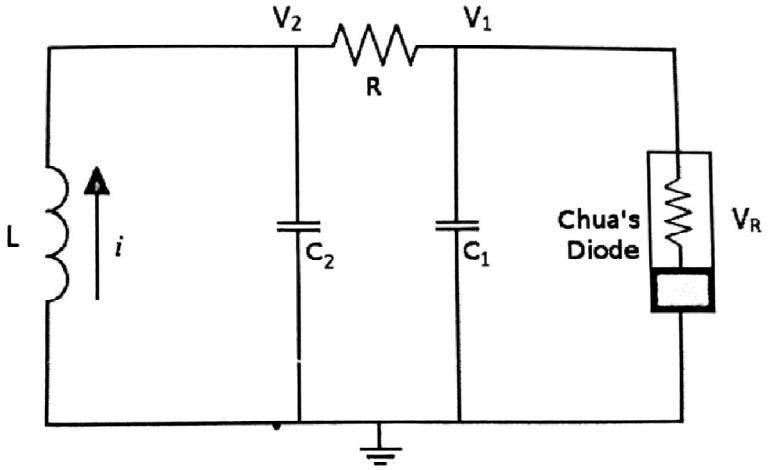

Figure 2

Classical Chua's circuit

2. Methodology

The present work is based on the following themes:

The first theme focuses on the properties of the circuit itself and analysis has been done on qualitative properties such as the bifurcation diagram[6], which depends on some control parameters.

The second theme focuses on alternative designs of Chua's circuit while the third theme includes a vast majority of the current research in thisfield,and featuresthe use of the Chua's circuit in different applications.

Based on these three themes we have realized the chaotic nature in Chua's circuit and checked those parameters which produced chaos in the oscillator and by varying the values of those parameters, limits have been found out up to which the oscillator shows its chaotic nature.

2.1 Componentsused to implement the circuit

The practical and classical Chua's circuits are presented in figures 1and2. Here the resistor is the most basic part of the electrical components. In order to have a good quality, we use metal film resistors[7]which should have a low noise, weak nonlinearity and relatively insensitive to temperature variations. The value of the resistances that has been used in our present circuit are 220 Ω, 1420 Ω, 2.2 $K\Omega$, 3.3 $K\Omega$,22 $K\Omega$. Apotentiometer[8] of resistance of 10 $K\Omega$ can be incorporated in the circuit.

Metalized polyester capacitors[9] are used because of their high quality and good electrical properties. The circuit needs capacitors whose magnitude is of the order 10-100nF[10].

An inductor has been used to implement the basic sinusoidal oscillator[11]. The value of inductor is 18 mH and the circuit is shown in fig 1 indicating the classical Chua's circuit.

2.2 Mathematical Model

From figure 2 we develop the relevant KCL and KVL equations as follows:

$$C_1 \frac{dV_1}{dt} = \frac{1}{R}(V_2 - V_1) - f(V_1) \quad \ldots (1)$$

$$C_2 \frac{dV_2}{dt} = \frac{1}{R}(V_2 - V_1) + i \quad \ldots (2)$$

$$L \frac{di}{dt} = -V_2 \quad \ldots (3)$$

Considering $G = 1/R$ we get,

$$\frac{dV_1}{dt} = \frac{1}{C_1 G(V_2 - V_1)} - \frac{1}{C_1} f(V_1) \quad \ldots (4)$$

$$\frac{dV_2}{dt} = \frac{1}{C_2 G(V_2 - V_1)} + \frac{1}{C_2 i} \quad \ldots (5)$$

$$\frac{di}{dt} = -\frac{V_2}{L} \quad \ldots (6)$$

The nonlinear term $f(V_1)$ is defined as,

$$f(V_1) = m_0 V_1 + \tfrac{1}{2}(m_1 - m_0)[|V_1 + E| - |V_1 - E|] \quad \ldots (7)$$

In figure 3, inputcharacteristics of Chua's diode is shown

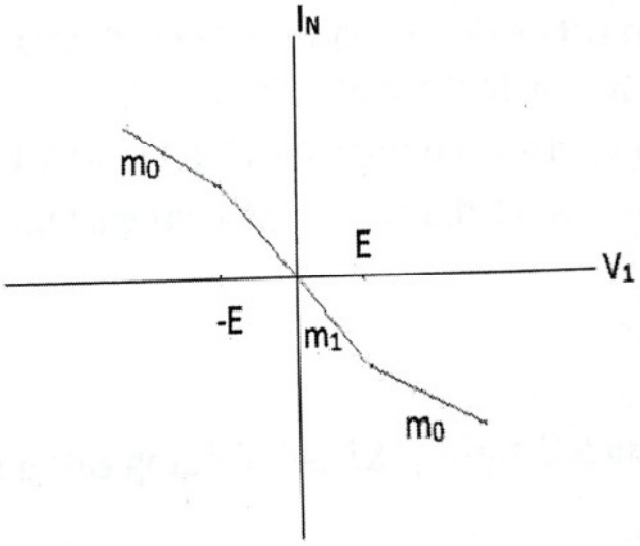

2.3 Dimensionless form of the equations

For easy computation, the dimensionless form of the above equations is presented here[12]

$\dot{x} = a[y - x - g(x)]$

$\dot{y} = x - y + z$

$\dot{z} = -by$

Where$\dot{x}, \dot{y}, \dot{z}$stand for the first order derivatives with respect to time and

$$g(x) = cx + \frac{1}{2}(d - c)[|x + 1| - |x - 1|]$$

the typical parameterschosen for the laboratory experiments are sfollows

$$R = 1420\,\Omega\,;\quad r = 63.8\,\Omega\,;\quad m_0 = -0.519\,;\quad m_1 = -0.865$$

$$E = 1.85\,V;\quad C_1 = 10.1\,nF;\quad C_2 = 101\,nf;\quad L = 20.8\,mH$$

Following the above dimensionless form, we have

$$a = 15;\quad b = 25.58;\quad c = -\frac{5}{7};\quad d = -\frac{8}{7}$$

3. Result and discussion

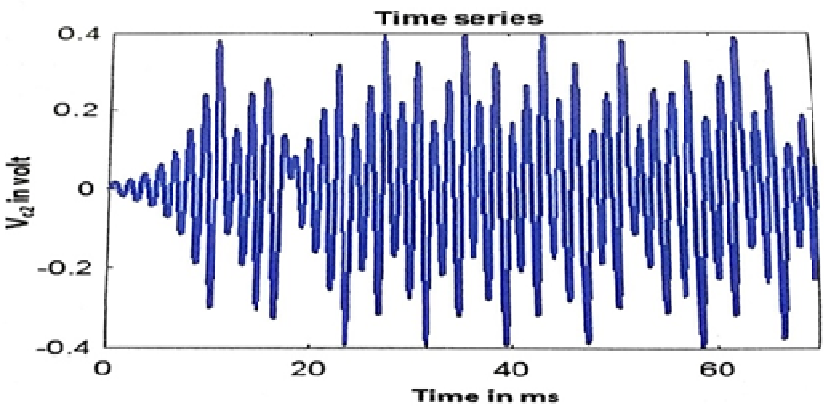

Figure 4

Time scale plot V_{c2} for experimental values of the of the parameter‘a’

The main output Vc_2 is shown in figure 4.The following case study has been carried out and discussed below.

The concept has been implemented in MATLAB ODE 45 and solved using RUNGE –FEHLBERG[13] method. Here, a graphical nature has been obtained by changing the parameters a, b, c, d.From the figure, it is observed that there are multiple frequency components and hence itcan be termed as multi period signal. Here are some examples of case studies by varying suitable parameterV_{C2}.

Case Study I:

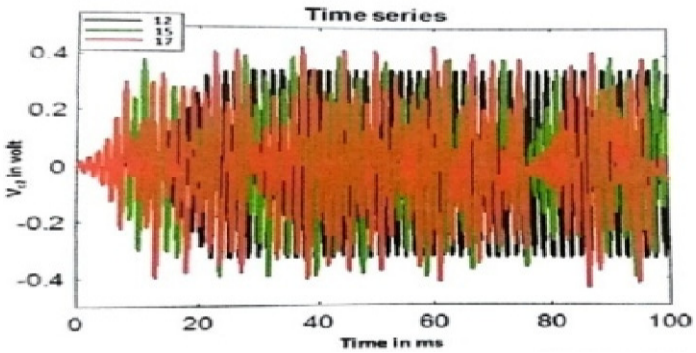

Figure 5(a)

Time scale plot of V_{c2} for the change in parameter'a'

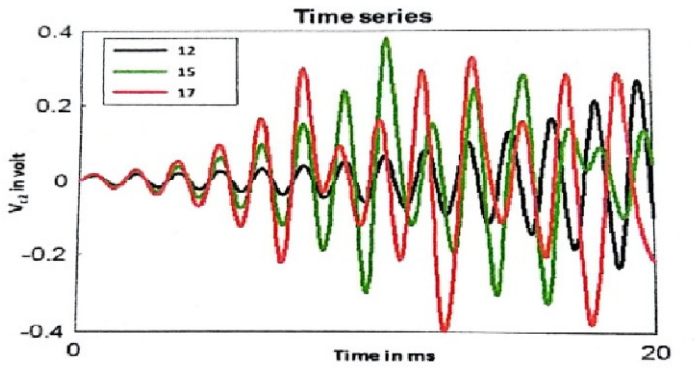

Figure 5(b)

Magnified time scale plot of V_{c2} for the change in parameter 'a'

Fig 5(a) is obtained by changing the parameter (a) only. Three sets of values are taken for 'a' i.e.12,15, 17 has been considered. Fig 5(b) is the magnified version of the previous one considering the time span from $0\ ms$ to $20\ ms$.

Case Study II:

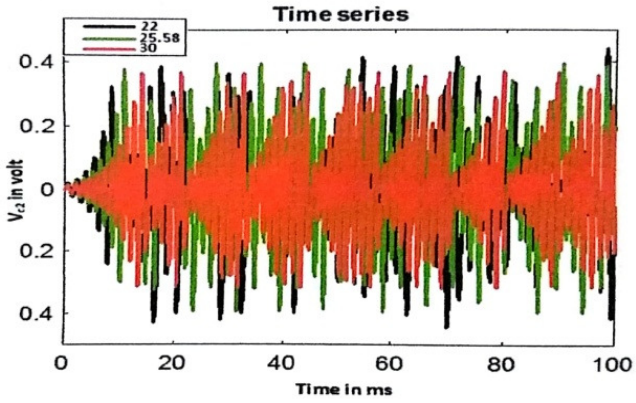

Figure 6 (a)

Time scale plot of V_{c2} for the change in parameter *'b'*

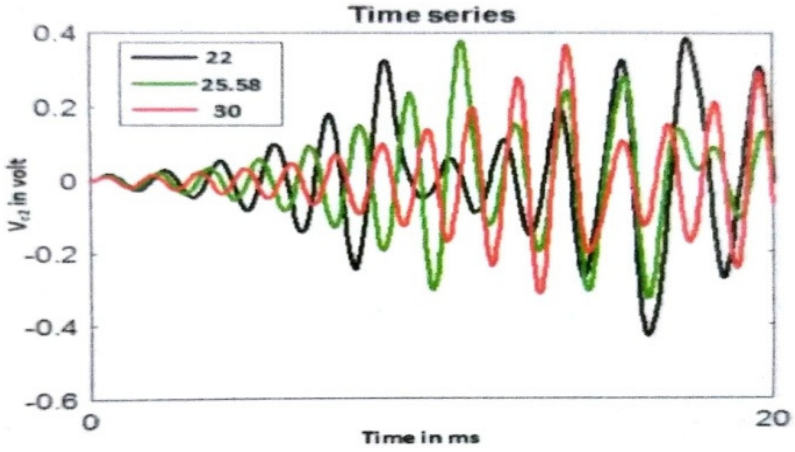

Fig 6 (b)

Magnified time scale plot of V_{c2} for the change in parameter *'b'*

Figure 6(a) is obtained by changing the parameter 'b' only. We have taken the sets of value of b i.e. 22, 25, 58, 30. Fig 6 (b) is the

magnified version of the previous one. The time span we have taken is from $0\ ms$to$20\ ms$.

Case study III

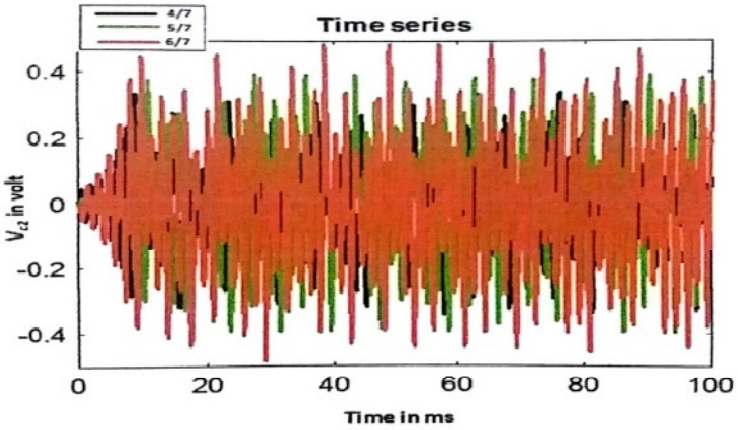

Figure 7 (a)

Time scale plot of V_{c2} for the change in parameter *'b'*

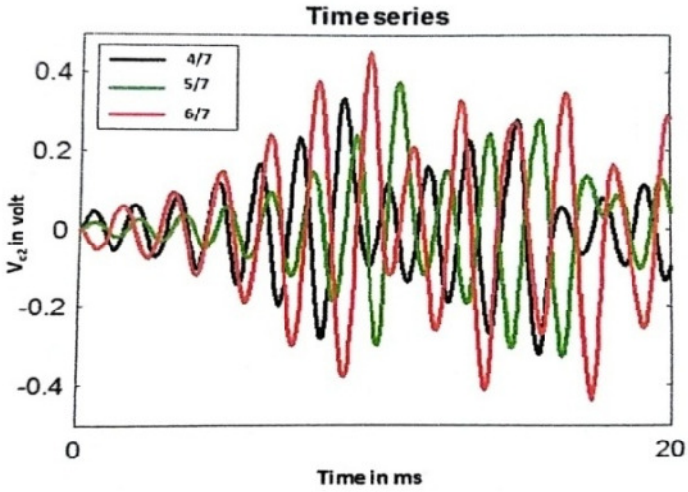

Figure 7 (b)

Magnified time scale plot of V_{c2} for the change in parameter *'b'*

Fig 7(a) is obtained by changing the parameter c only.Three sets of values have been considered for 'c' i.e 4/5, 5/7, 6/7 . Fig 7 (b) is the

magnified version of the previous one. The time span has been considered from $0\ ms$to $20\ ms$.

Case Study IV

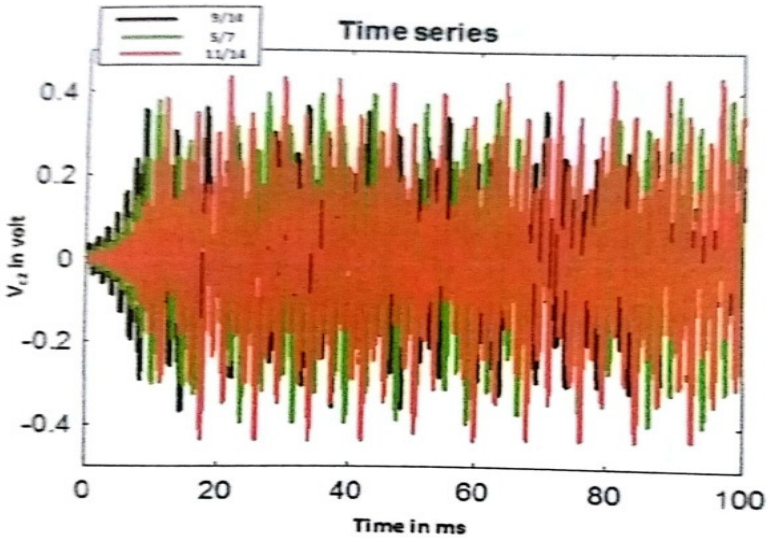

Figure 8 (a)

Time scale plot of V_{c2} for the change in parameter *'b'*

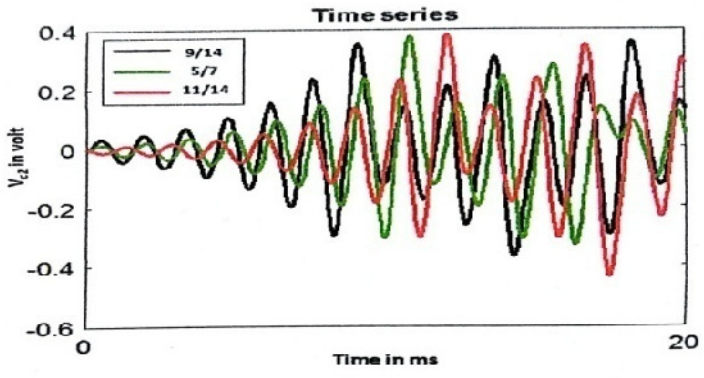

Figure 8 (b)

Magnified time scale plot of V_{c2} for the change in parameter *'b'*

Fig 8(a) is obtained by changing the parameter 'c' for other three sets of values i.e 9/14, 5/7, 11/14. Fig 8 (b) is magnified version of the previous one.The time span has been considered from 0 msto20 ms.

Case Study V

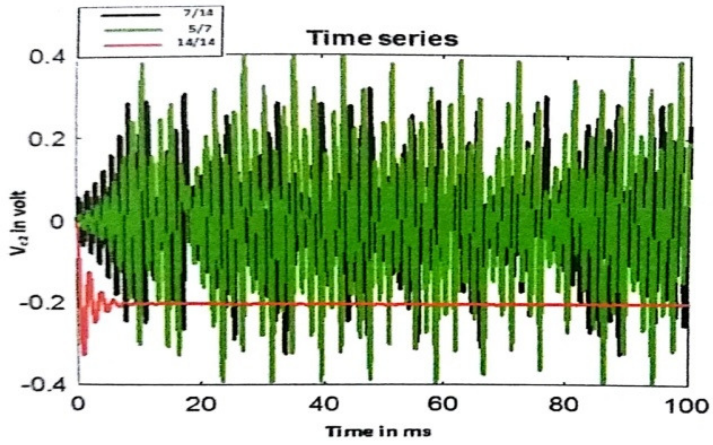

Figure 9 (a)

Time scale plot of V_{c2} for the change in parameter *'c'*

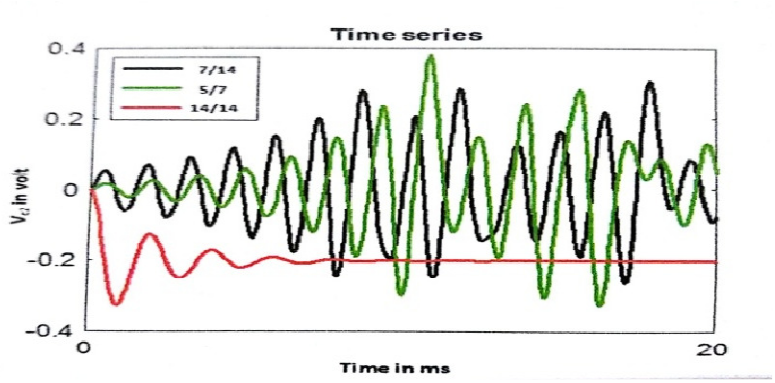

Figure 9 (b)

Magnified time scale plot of V_{c2} for the change in parameter *'c'*

Another graph has been simulated by varying the parameter 'c'. Three sets of considered values being 7/14, 5/7, 1 and time span has been considered from 0 $ms$to 20 ms.

We note the following general features of Chua's chaotic oscillator using Chua's circuit

As the nature of V_{c2} is highly sensitiveto the variation of the parameter'd', so a proper plot was not obtained.

The sum of the parameters 'c' and 'd' should be greater than or equal to -2. A little change in this value, will result in linearity.

(a) The nature of the curve changes with the change in *'a'*. A change in *'a'* means change of the equilibrium position.

(b) The change in *'c'* results in a change in the slope of the output of Chua's diode which also changes the nature of the curve.

5. Conclusion

In the present work on Chua's circuit, our main objective is to designany electronic oscillator which is chaotic and also to check those parameters which control the chaotic nature.

Here, our objective is to use Chua's diode which acts as non-linear resistance. This makes the LC oscillator chaotic. We used MATLAB simulation software to obtain the graphical nature of the output.

The time scale output curve of the parameter 'V_{c2}' shows multiple frequency components which is equivalent to multiple turns in Chua's double scroll attractor.From the output we can conclude that the oscillator no longer repeats any signal after a certain time period i.e. the nature of the output oscillation cannot be predicted.

Here we have obtained simulated results as well as practical results. The nature of the output in both the cases are similar. So, we can conclude that the output fairly agrees with our objectives.

Acknowledgements

This paper is the outcome of the M. Tech. project work of S. Das. Thanks are due to Electrical Engineering Department of Narula Institute of Technology for providing the MATLAB facilities.

References

1. Gleick J., Chaos, Vintage Books UK (2011).
2. Ross S. M., Stochastic Processes, Willey India (2008).
3. ChuaandG. Lin L. O., IEEE trans circuits system **137**, 885(1990).
4. Kabel A. C., Proceedings of the 2003 Particle Accelerator Conference **4** (2003).
5. Boyelestad R. L. and Nashelsky L., Electronic devices and circuits, Pearson Education, New Delhi (2015).
6. Awerejcewicz J., Bifurcation and Chaos, Springer (2011)
7. Berkin A. B. and Sokolov Y. V.,5th Korea-Russia International Symposium on Science and Technology. Proceedings. KORUS 2001 (Cat. No.01EX478) **1** (2001).
8. Demurie S. and Mey G. D.,IEEE Transactions on Instrumentation and Measurement 38, issue-3, (1989).
9. Qi-guo Y., Fourth International Conference on Intelligent Computation Technology and Automation, **2,** (2011).
10. Beal A. N., Bailey J. P., Hale S. A., Dean Hamilton R. N., M., Tugnait J. K., Hahs D. W. and Corron N. J., MILCOM 2012 - 2012 IEEE Military Communications Conference, (2012).

11. Voliansky R., SadovoiandA., Shramko Y., International Scientific Practical Conference Problems of InfocommunicationsScience and technology (PIC S&T) (2018).
12. Elwakil A. S. and Kennedy M. P., Journal of Franklin Institute **337**, 251 (2000)
13. Pal S., Numerical methods, Oxford University press, New Delhi (2009)

———————

INDIAN JOURNAL OF THEORETICAL PHYSICS, VOL 68, NOS. 1 & 2, 2020

Effect of Slip Velocity on Polar Fluid Model of Blood Flow in Large Vessels

Jitesh Kumar Singh

Assistant Professor, Department of Mathematics,

T. D. Post Graduate College, Jaunpur – 222002 (U. P.) India.

[Abstract : Observation indicates that slip of the wall affects axial velocity where as rotational velocity is unaffected. The effects of velocity slip on the apparent viscosity were studied and the restrictions on slip for the occurrence of sigma phenomenon are obtained. Further, the variations of velocity profiles and pressures gradient are shown graphically.]

Key words : Slip Velocity, Polar Fluid Model and Sigma phenomenon.

1. Introduction

The question of slip in fluid dynamics has been pondered for some time in the study of rheology of blood and other non-Newtonian fluids. Blood, a class of fluid has its components as plasma, platelets, erythrocytes and leukocytes, but most of its rheological properties depend on RBC (Red Blood Cell), which in normal condition occupy some 40 – 45% fraction of total blood volume. The existence of the suspended particles influences the properties of the suspension in bulk and in particular its viscosity is increased. It has recently been shown that many of the non-Newtonian phenomenons associated with fluid suspension can be described by means of the theory of structured

continua. For fluid suspensions of relatively high concentration, particle interactions become important. These interactions give rise to substructure spin and deformation gradient. When these gradients are neglected, the theoretical model provides results consistent with experimental findings of dilute suspensions. By retaining S as a wall effect parameter, a simple shear flow is considered and an expression for the relative viscosity is obtained. Arguments were presented showing S to be related to the suspension concentration C_s, and the simple relation between the two quantities was postulated.

In the present paper we consider the problem of Poiseuille flow of a suspension with rigid spherical substructure. A continuum model whose substructure corresponds to the particle in suspension is considered. The constitutive equations for this continuum which is a polar fluid have been advanced from different point of view by Ariman *et al.*[1], Brunn[2], Chaturani[4], Cowin[5], Erdogen[7], and Kline *et al.*[9]. Further, Nishad *et a1*[17], Jyoti *et a1*[16], and Singh, *et al*[12 ,13,14,15] have enriched the literature by their contributions. They have given several suggestions for boundary conditions to be employed with the governing equations. It has been shown by Goldsmith[8] and Kline *et al.*[9] that physical arguments indicate a connection between suspension concentration and choice of particle spin boundary condition. As far as fluidity is concerned, one may in this limit approximate the polar fluid by a Newtonian one provided that corresponding boundary condition of slip velocity is employed. By using the example chosen by Ebert[6] to compare theory and experiment, it is demonstrated that the slip parameter can be adjusted such that the excellent agreement results.

The quantitative behaviour of the experiment in which the increase of the apparent fluidity with decreasing dimensions of the vessel was found to be of general occurrence in suspension rheology[8]. A positive slip coefficient guarantees this behaviour to result. In the important limit in which the length scale of the microstructure is much less than the characteristic length, the Navier – Stokes equations subject to velocity slip boundary condition are well that one has to work with for the evaluation of apparent fluidity. According to Brunn[2], the requirement of velocity slip is a natural and physically expected supposition for any continuum approximation of a fluid with internal structures. In view of the argument stated above, we have proposed to apply velocity-slip and spin in angular velocity at the wall.

The Mathematical Model : We consider an incompressible fluid flowing in a circular tube of radius R, and restrict the discussion to a rigid spherical substructure. The flow is considered to be steady, fully developed and laminar. The equations of motion for an incompressible polar fluid flow neglecting body forces and body couples for Poiseuille flow are

$$\frac{(\mu + \tau)}{r} \frac{d}{dr}\left(r \frac{dv}{dr} \right) + \frac{2\tau}{r} \frac{d}{dr}(r\omega) - \frac{\partial p}{\partial z} = 0 \qquad \text{... (1)}$$

$$\frac{\partial P}{\partial r} = \frac{\partial P}{\partial \theta} = 0 \qquad \text{... (2)}$$

$$\gamma \frac{d}{dr}\left[\frac{1}{r} \frac{d}{dr}(r\omega) \right] - 4z\left[\omega + \frac{1}{2} \frac{dv}{dr} \right] = 0 \qquad \text{... (3)}$$

where (0, 0, $v(r)$) is the velocity; $\omega(r)$ the total angular velocity; r, z the radial and axial co-ordinates; P the pressure; μ the shear viscosity; τ the rotational viscosity; γ the viscosity of the gradient of particle angular velocity, R is tube radius. To solve the equations (1) and (2) we apply

slip in axial and angular velocities at the wall and their finite values at the axis.

The boundary conditions then take the from

$$v(R) = \frac{1}{4\mu\ v_s}\left(\tau_{rz} - \tau_{zr}\right), \quad \omega(R) = \frac{1}{4\mu\ B_t}\left(\tau_{rz} - \tau_{zr}\right) \qquad \ldots (4)$$

where v_s = suspension velocity, B_t = boundary parameter

and $\quad v(0) = 0, \qquad \omega(0) = 0. \qquad \ldots (5)$

The expressions for shear stress τ_{rz} and τ_{zr} are obtained as, Prnnington and Cowin[10]

$$\tau_{rz} = (\mu - \tau)\frac{dv}{dr} - 2\tau\omega \qquad \ldots (6)$$

$$\tau_{zr} = (\mu + \tau)\frac{dv}{dr} + 2\tau\omega \qquad \ldots (7)$$

In view of (6) and (7), boundary conditions (4) and (5) can be written in the form

$$v(R) = -\frac{\sigma}{2}\frac{dv}{dr}, \quad \omega(R) = -\frac{S}{2}\frac{dv}{dr}, \quad v(0) = 0, \quad \omega(0) = 0 \qquad \ldots (8)$$

$$\text{where } \sigma = \frac{\tau}{\tau + \mu\, v_s}, \qquad S = \frac{\tau}{\tau + \mu\, B_t}. \qquad \ldots (9)$$

Solutions of equations (1) and (3) subject to boundary condition (8) are

$$v(\xi) = -\frac{dp}{dz}\frac{R^2}{4\mu}\left[1 - \xi^2 - 2\eta\,\bar{S}\left\{\frac{I_0(\lambda) - I_0(\lambda\xi)}{\lambda\ I_1(\lambda)}\right\} + 2\chi(1 - \eta\,\bar{S})\right] \qquad \ldots (10)$$

$$\text{and} \quad \omega(\xi) = -\frac{dp}{dz}\frac{R}{4\mu}\left[\xi - \bar{S}\,\frac{I_1(\lambda\xi)}{I_1(\lambda)}\right] \qquad \ldots (11)$$

$$\left.\begin{aligned} &\text{where } \xi = \frac{r}{R}, \quad \chi = \frac{\sigma}{2R}, \quad \lambda^2 = \frac{4R^2\,\tau\mu}{\gamma(\tau + \mu)} \\ &\eta = \frac{\tau}{\tau + \mu}, \quad \bar{S} = \frac{1 - S}{1 - \eta S}, \quad (0 \le \bar{S} \le 1) \end{aligned}\right\} \qquad \ldots (12)$$

In the modified Bessel functions of order n.

Furthermore, we note that

$$\tau \leq 0, \quad \gamma \leq 0, \quad \tau + \mu \geq 0. \qquad \text{... (13)}$$

From the equation (10), we obtained the volumetric flow rate Q as

$$Q = \int_0^R 2\pi r \, v \, dr$$

$$\text{or } Q = \frac{\pi R^4 K}{8\mu}\left[1 - 4\eta\bar{S}\left\{\frac{\lambda I_0(\lambda) - 2I_1(\lambda)}{\lambda^2 I_1(\lambda)}\right\} + 4\chi\left(1-\eta\bar{S}\right)\right] \qquad \text{... (14)}$$

$$\text{If,} \qquad \mu_a = \frac{\pi R^4 K}{8Q} \qquad \text{... (15)}$$

$$\text{then} \quad \mu_a = \mu\left[1 - 4\eta\bar{S}\left\{\frac{\lambda I_0(\lambda) - 2I_1(\lambda)}{\lambda^2 I_1(\lambda)}\right\} + 4\chi\left(1 - \eta\bar{S}\right)\right]^{-1} \qquad \text{... (16)}$$

Velocity at the axis of the tube is obtained from equation (10) in the form given by

$$V_a = \frac{KR^2}{4\mu}\left[1 - 2\eta\bar{S}\left\{\frac{I_0(\lambda) - 1}{\lambda I_1(\lambda)}\right\} + 2\chi\left(1-\eta\bar{S}\right)\right] \qquad \text{... (17)}$$

2. Discussion

We may discuss the effect of volume concentration of suspended rigid particles in the Poiseuille flow problem by eq. (14). It is quite pertinent that the results obtained above can be applied to explain the influence of volume concentration of red cells in blood flow through large vessels. We may assume that the deformable nature of blood cells is relatively unimportant in understanding the blood flow in large diameter vessels.

If we put $$H = 4\left[\frac{\lambda\ I_0(\lambda) - 2\ I_1(\lambda)}{\lambda^2\ I_1(\lambda)}\right] \quad \ldots (18)$$

then $$\mu_a = \mu\left[1 - \eta\,\bar{S}\,H + 4\chi\left(1 - \eta\,\bar{S}\right)\right]^{-1}; \quad 0 \le H \le 1; \quad 0 \le \bar{S} \le 1 \quad \ldots (19)$$

Equations (10) and (11) show that slip in velocity at the wall affects the axial velocity whereas the angular velocity remains unaffected. For slip parameter $\chi = 0$, the apparent viscosity increases provided $\eta\,\bar{S}\,H \to 1$ ($\eta << 1$ always for viscous suspension), i.e. the two factors tend to their maximum values, as $H \to 1$ when $\lambda \to 0$ and $\bar{S} \to 1$ when $S \to 0$. Thus, H assumes the higher values when tube radius decreases and so we have the Inverse Fahraeus – Lindqvist result. Vand[11] has shown experimentally that apparent viscosity is a monotonic increasing function of suspension concentration $\bar{S}$. From equation (19), we see that the introduction of slip in axial velocity at wall still help Inverse Fahraeus – Lindqvist effect to exist. In Brunn[2] analysis equation.

$$\mu_a = \mu_s\left[1 + 2\left\{C_1\frac{L^2}{R^2}\ I_1\ \frac{(2\ N\ R)}{\ell} - C_0\right\}\right]^{-1},$$

$\mu_a < \mu_s$ does not give sigma effect (Fahraeus – Lindqvist Effect), instead for sigma effect to occur restriction should be $\left\{C_1\frac{\ell^2}{R^2}I_1\left(\frac{2\,N\,R}{\ell}\right) - C_0\right\}$ to decrease when the tube radius increases , i.e. C_0 (the slip parameter) to increase when tube radius increases. Thus the concentration increases with increasing tube radius meaning that apparent viscosity increases with tube radius, a trend of Fahraeus – Lindqvist effect. The equation (19) shows that even a small positive value of χ decreases μ_a. From the graphs and excremental values of Bugliarello and Sevilla[3], we have extrapolated a table which shows that χ increases with $\bar{S}$, a result which has not yet been obtained by previous authors in the field. Taking help of Vand[11] analysis, it can be concluded that the increase in χ results an

increase in μ_a. This also supports the "IFLE" (Inverse Fahraeus – Lindquist Effect). Our conclusion is well supported by Chaturani and Biswas[4] in which they have proved that Brunn[2] statement of velocity slip to help sigma effect is erroneous.

The boundary condition parameter B_t of Brunn[2] analysis is related with S by

$$B_t = \left(\frac{1}{S} - 1\right)\frac{\tau}{\mu}\,; \qquad B_t \geq 0.$$

For the discussion we have considered two different cases :

In case – I we suppose $\mu = \mu_s + \tau$ and in case – II we suppose $\mu = \mu_s$ as solvent viscosity. We observe that the results obtained for case – I are in conformity of the experimental values, whereas the results of case – II are in parity to the results of Erdogen[7] analysis which when compared to the experimental values give unsatisfactory readings. For 40% concentration and 40 μ_m tube, we have used the data of Ariman *et al.* [2] as $\mu_s = 1.2\ C_p$, $\tau = 0.98\ C_p$, $\gamma = 12 \times 10^{-8}\ g_m\ C_m$/Sec. and for experimental verification, the data of Bugliarello and Sevilla[3] were used. For different values of $\bar{S}$ and χ, the values of μ_a, V_a, $-\frac{dp}{dz}$, $v(\xi)$ and $\omega(\xi)$ are shown in Tables (1 – 5). For $\chi = 0.02$, the apparent viscosity μ_a varies from 2.02 to 2.88 whereas for $\chi = 0$ this range is from 2.18 to 3.109 which is greater than the previous one. From the analysis of Bugliarello and Sevilla[3] the experimental value of μ_a for 40% concentration could be read anywhere between 2.1 and 2.5. Here, we have chosen the value of μ_a arbitrarily equal to 2.5. We are not known with any precise experimental value of $\bar{S}$, only it can be estimated from eqn. (16) as in it other quantities except $\bar{S}$ can be experimentally known. The values of $\bar{S}$ lying between 0.35 and 0.66 give better theoretical results. We can

approximate $\bar{S} \approx 0.5$, because for this value of $\bar{S}$ there are small errors in μ_a and V_a when compared with experimental values. V_s is suspension velocity.

Variation of pressure gradient and axial velocity with respect to χ and $\bar{S}$ are reported in Table (2). Variations of velocity and rotation profiles for different $\bar{S}$ are shown in Tables (3 and 4). From Tables we observe that when $\bar{S}$ increases, particles axial and rotational velocities decrease. If $\bar{S}$ is assumed to be the measure of concentration, then it is seen that for dilute suspension, particles rotation increases with tube radius (a case of Newtonian fluid). But for sufficiently large values of $\bar{S}$ ($\bar{S} > 0.85$) the rotation at first increases, attains its maximum value and then decreases near the wall. For maximum concentration ($\bar{S} = 1$) the particle rotation is maximum at $\frac{r}{R} \simeq 0.75$ which has been experimentally observed.

Table 1

Variation of μ_a, V_a and V_S for Different Values of $\bar{S}$, for 40% Concentration and in 40 μ_m Tube.

χ	$\bar{S}$	μ_a	V_a	V_S
0.02	0	2.02	3.11	0.119
0.02	0.265	2.19	2.085	0.109
0.02	0.350	2.25	2.79	0.106
0.02	0.491	2.36	2.66	0.101
0.02	0.52	2.39	2.63	0.100
0.02	0.666	2.52	2.50	0.095
0.02	1.000	2.88	2.20	0.082

Table 2

Variation of $-\frac{dp}{dz}$, V_a and V_S with respect to χ and $\bar{S}$, for 40% Concentration and in 40 μ_m Tube.

χ	$\bar{S}$	$-\frac{dp}{dz}$	V_a	V_S
0.01	0.591	65.31	2.47	0.048
0.02	0.591	64.27	2.53	0.097
0.02	0.591	64.27	2.57	0.097
0.02	0.591	61.37	2.66	0.101
0.05	0.591	60.32	2.67	0.244

Table 3

Variation of Velocity Profiles for Various Values of $\bar{S}$, $\chi = 0.02$ for 40% RBC Concentration and in 40 μ_m Tube.

y	V(y)				
	$\bar{S} = 0$	$\bar{S} = 0.35$	$\bar{S} = 0.5$	$\bar{S} = 0.66$	$\bar{S} = 1.0$
0.0	3.112	2.795	2.657	2.504	2.199
0.2	2.996	2.687	2.554	2.407	2.112
0.4	2.637	2.363	2.245	2.115	1.854
0.6	2.037	1.823	1.731	1.629	1.425
0.8	1.199	1.070	1.015	0.955	0.833
1.0	0.199	0.106	0.101	0.094	0.082

Table 4

Variation of Particles Rotational Velocity with $\overline{S}$, 40% Concentration and 40 μ_m Tube.

y	$\overline{S}$						
	0.00	0.35	0.50	0.66	0.75	0.85	1.00
0.0	0.0	0.0000	0.0000	0.0000	0.0000	0.0000	0.0000
0.2	0.2	0.1372	0.1102	0.0804	0.0652	0.0472	0.0203
0.4	0.4	0.2725	0.2178	0.1573	0.1266	0.0901	0.0351
0.6	0.6	0.4043	0.3204	0.2276	0.1806	0.1247	0.0408
0.8	0.8	0.5309	0.4159	0.2878	0.2232	0.1463	0.0309
1.0	1.0	0.6500	0.5000	0.3400	0.2500	0.1500	0.0000

Table 5

Variation of Apparent Viscosity and Axial Velocity for Different $\overline{S}$, for 40% Concentration and in 40 μ_m Tube.

χ	$\overline{S}$	μ_a	V_a	V_S
0.02	0.000	1.11	5.66	0.217
0.02	0.350	1.31	5.35	0.183
0.02	0.500	1.42	4.44	0.168
0.02	0.666	1.56	4.03	0.152
0.02	1.000	1.97	3.22	0.119

References :

1. Ariman, T.; Turk, M. A. and Sylvester, N. D.: Steady and Pulsatile Flow of Blood. J. Appl. Mech. ASME, **41**, 1(1974).
2. Brunn, P.: The velocity Slip of Polar Fluids. Rheologica Acta, **14,** 1039(1975).
3. Bugliarello, G. and Sevilla, J.: Velocity Distribution and other Characteristics of Steady and Pulsatile Blood Flow in Fine Glass Tubes. Biorheology, 7, 85(1970).
4. Chaturani, P. and Biswas, D.: A Comperative Study of Poiseuille flow of a Polar Fluid Under Various Boundary Conditions with Application to Blood Flow. Rheologica Acta, **23**, 435 (1984).
5. Cowin, S. C.: On the Polar Fluid as a Model for Blood Flow in Tubes. Biorheology**, 9**, 23 (1972).
6. Ebert, F.: Rheologica Acta, **14**, 258 (1975).
7. Erdogen, M. E.: Polar Effects in Apparent Viscosity of Suspension. Rheologyca Acta, 9, 434 (1980).
8. Goldsmith, H. L.: "Deformation of human red cells in tube flow". Biorheology, **7,** 235 – 245 (1971).
9. Kline, K. A.; Allen, S. J. and DeSilva, C. N.: A Continuum Approach to Blood Flow. Biorheology, **5,** 111 (1968).
10. Pennington, C. J. and Cowin, S. C.: Trans. Soc. Rheol., **14**, 219 (1970).
11. Vand, V.: Jour. Phys. Colloid Chem., **52**, 300 (1948).
12. Singh, N.L. and Vidita. Analysis of the blood flow behaviour in narrow tapered tube through non-linear mathematical model. Jour. PAS **23**, 58-66**,** (2011).
13. Singh, N.L., Singh, Jitesh Kumar, Shukla, A and Asthana, V., Effect of slip on viscous resistance experienced by a non-Newtonian fluid model. Jour. PAS, **19,** 95-98 (2013).
14. Singh, Jitesh Kumar. Blood rheology interpreted through core and discharge hematocrit in narrow capillaries. Jour. PAS, **14**, 303-308, (2008).

15. Singh, N.L. and Singh Jitesh Kumar. Mathematical study of steady blood flow in narrow vessel w3ith plasma layer near the wall. Indian Jour. of Theoretical Physics, **50**, 2, (2002).
16. Mishra, J., Singh, Jitesh Kumar and Singh, N.L.. A rheological fluid model for magnetohydrodynamic paralled plates hemodialyser. Acta Cincia Indica, XXXM, No. **1**, 149, (2004).
17. Nishad Vidita, Singh, N.L. and Pandey, A.K.. Effect of particles concentration on fluid viscosity represented by different models. Indian Jour. of Theoretical Physics, **60**, 136, (2012).

———

INFORMATION TO AUTHORS

Manuscripts should represent results of original works on theoretical physics or experimental physics with theoretical background or on applied mathematics. Letters to the Editor and Review articles in emerging areas are also published. Submission of the manuscript will be deemed to imply that it has not been published previously and is not under consideration for publication elsewhere (either partly or wholly) and further that, if accepted, it will not be published elsewhere. It is the right of the Editorial Board to accept or to reject the paper after taking into consideration the opinions of the references.

Manuscripts may be submitted in pdf/MS word format to **admin@citphy.org or susil_vcsarkar@yahoo.co.in** Online submission of the paper through our **website: www.citphy.org** is also accepted. The file should be prepared with 2.5 cm margin on all sides and a line spacing of 1.5.

The title of the paper should be short and self-explanatory. All the papers must have an abstract of not more than 200 words, the abstract page must not be a part of the main file. Abstract should be self-contained. It should be clear, concise and informative giving the scope of the research and significant results reported in the paper. Below the abstract four to six key words must be provided for indexing and information retrieval.

The main file should be divided into sections (and sub-sections, if necessary) starting preferably with introduction and ending with conclusion. Displayed formula must be clearly typed (with symbols defined) each on a separate line and well-separated from the adjacent text. Equations should be numbered with on the right-hand side consecutively throughout the text. Figures and Tables with captions should be numbered in Arabic numerals in the order of occurrence in the text and these should be embedded at appropriate places in the text. Associated symbols must invariably follow SI practice.

References should be cited in the text by the Arabic numerals as superscript. All the references to the published papers should be numbered serially by Arabic numerals and given at the end of the paper. Each reference should include the

author's name, title, abbreviated name of the journal, volume number, year of publication, page numbers as in the simple citation given below :

For Periodicals : Sen, N. R. - On decay of energy spectrum of Isotopic Turbulence, 1. Appl. Phys. **28,** No. 10, 109-110 (1999).

1. Mikhilin, S. G. - Integral Equations, Pergamon Press, New York (1964).
2. Hinze, A. K. - Turbulence Study of Distributed Turbulent Boundary Layer Flow, Ph. D, Thesis, Rorke University (1970).

The corresponding author will receive page proof, typically as a pdf file. The proof should be checked carefully and returned to the editorial office within two or three days. Corrections to the proof should be restricted to printing errors and made according to standard practice. At this stage any modifications (if any) made in the text should be highlighted.

To support the cost of publication of the journal, the authors (or their Institutions) are requested to pay publication charge ₹ 200/- per printed page for authors of Indian Institutes and US$ 20 for others. Publication charges to be sent directly to **CALCUTTA INSTITUTE OF THEORETICAL PHYSICS, 'BIGNAN KUTIR', 4/1 MOHAN BAGAN LANE, KOLKATA-700004, INDIA.**

A pdf of the final publisher's version of the paper will be sent to the corresponding author.

All communications are to be sent to the Secretary, Calcutta Institute of Theoretical Physics, 'Bignan Kutir', 4/1, Mohan Bagan Lane, Kolkata-700004, India. E-mail: susil_vcsarkar@yahoo.co.in

For details please visit our website www.citphy.org

INDIAN JOURNAL OF THEORETICAL PHYSICS

International Board of Editorial Advisors

B. Das Gupta, (*USA*)
Nao-Aki Noda, (*Japan*)
D. S. Roy, (*India*)
A. Sen, (*India*)
A. Roy Chaudhury, (*India*)
S. Raha, (*India*)
A. H. Siddiqi, (*India*)
N. K. Gupta, (*India*)
K. Ghatak, (*India*)
O.P. Agarwal, (*USA*)
Ching-Kong Chao, (*Taiwan*)
M. R. Islami, (*Iran*)
Halina Egner, (*Poland*)
K. C. Deshmukh, (*India*)
A. Kundu, (*India*)
B. Chakraborty, (*India*)
A. N. Sekhar Iyengar, (*India*)
J. K. Bhattacharjee (*India*)

BOARD OF EDITORS

J. K. Bhattacharjee
M. Chakraborti
S. K. Biswas
R. K. Bera
D. Syam
I. Bose
M. Kanoria
P. R. Ghosh
Rita Chaudhuri
S. K. Sarkar
D. C. Sanyal
P. K. Chaudhuri
D. Sarkar
A. Sanyal
J. Mukhopadhyay
A. K. Ghosh

Editorial Secreatry : D. C. Sanyal

CALCUTTA INSTITUTE OF THEORETICAL PHYSICS

(Formerly, Institute of Theoretical Physics)

[Established in 1953 by Late Prof. K. C. Kar, D. Sc.]

Director and President : J. K. Bhattacharjee
Vice-President : P. R. Ghosh
Secretary : S. K. Sarkar
*Asst. Sec*retary : P. S. Majumdar
Members : A. Roy, M. Kanoria, D. C. Sanyal, J. Mukhopadhyay, M. Chakraborti

PUBLICATIONS
OF
CALCUTTA INSTITUTE OF THEORETICAL PHYSICS
"BIGNAN KUTIR"
4/1, Mohan Bagan Lane, Kolkata-700 004, India
Phone : +91-33-25555726

INDIAN JOURNAL OF THEORETICAL PHYSICS (ISSN : 0019-5693)
Research Journal containing Original Papers, Review Articles and Letters to the Editor is published quarterly in March, June, September and December and circulated all over the world.

Subscription Rates
₹ 1500 per volume (for Bonafide Indian Party)
US$ 350 (for Foreign Party)

Back Volume Rates
₹ 1500 per volume (for Bonafide Indian Party)
US$ 350 per volume or Equivalent Pounds per volume

Books Written by Prof. K. C. Kar, D. Sc.

- **INTRODUCTION TO THEORETICAL PHYSICS [Vol. I and Vol. II (Accoustics)]** Usefull to students of higher physics
  Price : ₹ 60 or US $ 10 per volume
- **WAVE STATISTICS : Its principles and Applications [Vol. I and Vol. II]** Usefull to Post Graduate and Research students
  Price : ₹ 80 or US $ 12
- **STATISTICAL MECHANICS : PRINCIPLES AND APPLICATIONS [Vol. I and Vol. II]** Usefull to Advanced students of theoretical Physics
  Price : ₹ 120 or US $ 15
- **A NEW APPROACH TO THE THEORY OF [Vol. I and Vol. II]** Usefull to Post Graduate and aDVANCED students
  Price : ₹ 50 or US $ 8

Order may be sent directly to Calcutta Institute of Theoretical Physics
"Bignan Kutir", 4/1, Mohan Bagan Lane, Kolkata-700 004, India

---

All rights (including Copyright) reserved by the Calcutta Institute of theoretical Physics. and published by Dr. S. K. Sarkar, Secretary, on behalf of Calcutta Institute of Theoretical Physics, 4/1, Mohan Bangal Lane, Kolkata- 700 004, India.